Practical Rateless Set Reconciliation

Lei Yang[1] Yossi Gilad[2] Mohammad Alizadeh[1]

[1]MIT CSAIL [2]Hebrew University of Jerusalem

ABSTRACT

Set reconciliation, where two parties hold fixed-length bit strings and run a protocol to learn the strings they are missing from each other, is a fundamental task in many distributed systems. We present Rateless Invertible Bloom Lookup Tables (Rateless IBLT), the first set reconciliation protocol, to the best of our knowledge, that achieves low computation cost and near-optimal communication cost across a wide range of scenarios: set differences of one to millions, bit strings of a few bytes to megabytes, and workloads injected by potential adversaries. Rateless IBLT is based on a novel encoder that incrementally encodes the set difference into an infinite stream of coded symbols, resembling rateless error-correcting codes. We compare Rateless IBLT with state-of-the-art set reconciliation schemes and demonstrate significant improvements. Rateless IBLT achieves 3–4× lower communication cost than non-rateless schemes with similar computation cost, and 2–2000× lower computation cost than schemes with similar communication cost. We show the real-world benefits of Rateless IBLT by applying it to synchronize the state of the Ethereum blockchain, and demonstrate 5.6× lower end-to-end completion time and 4.4× lower communication cost compared to the system used in production.

1 INTRODUCTION

Recent years have seen growing interest in distributed applications, such as blockchains [1, 22, 36], social networks [27], mesh messaging [26], and file hosting [34]. In these applications, *nodes* (participating servers) maintain replicas of the entire or part of the application state, and synchronize their replicas by exchanging messages on a peer-to-peer network.

The naive approach to solving this problem requires communication proportional to the size of the set one party holds. For example, some applications send the entire set while other applications have parties exchange the hashes of their items or a Bloom filter of their sets (the Bloom filter's size is proportional to the set size). A node then requests the items it is missing. All these solutions induce high overhead, especially when nodes have large, overlapping sets. This is a common scenario in distributed applications, such as nodes in a blockchain network synchronizing transactions or account balances, social media servers synchronizing users' posts, or a name system synchronizing certificates or revocation lists [32].

An emerging alternative solution to the state synchronization problem is *set reconciliation*. It abstracts the application's state as a set and then uses a reconciliation protocol to synchronize replicas. Crucially, the overhead is determined by the *set difference* size rather than the set size, allowing support for applications with very large states. However, existing set reconciliation protocols suffer from at least one of two major caveats. First, most protocols are parameterized by the size of the set difference between the two participating parties. However, in practice, setting this parameter is difficult since scenarios such as temporal network disconnections or fluctuating load on the system make it challenging to know what the exact difference size will be ahead of time. Thus, application designers often resort to running online estimation protocols, which induce additional latency and only give a statistical estimate of the set difference size. Such estimators are inaccurate, forcing the application designers to tailor the parameters to the tail of the potential error, resulting in high communication overhead. The second type of caveat is that some set reconciliation protocols suffer from high decoding complexity, where the recipient has to run a quadratic-time or worse algorithm, with relatively expensive operations.

We propose a *rateless* set reconciliation scheme called Rateless Invertible Bloom Lookup Tables (Rateless IBLT) that addresses these challenges. In Rateless IBLT, a sender generates an infinite stream of *coded symbols* that encode the set difference, and the recipient can decode the set difference when they receive enough coded symbols. Rateless IBLT has no parameters and does not need an estimate of the set difference size. With overwhelming probability, the recipient can decode the set difference after receiving a number of coded symbols that are proportional to the set difference size rather than the entire set size, resulting in low overhead. Rateless IBLT's coded symbols are *universal*. The same sequence of coded symbols can be used to reconcile any number of differences with any other set. Therefore, the sender can create coded symbols once and use them to synchronize with any number of peers. The latter property is particularly useful for applications such as blockchain peer-to-peer networks, where nodes may synchronize with multiple sources with overlapping states, since it allows the node to recover the union of their states using coded symbols it concurrently receives from all of them.

In summary, we make the following contributions:

(1) The design of Rateless IBLT, the first set reconciliation protocol that achieves low computation cost and near-optimal communication cost across a wide range of scenarios: set differences of one to millions, bit strings of

a few bytes to megabytes, and workloads injected by potential adversaries.

(2) A mathematical analysis of Rateless IBLT's communication and computation costs. We prove that when the set difference size d goes to infinity, Rateless IBLT reconciles d differences with $1.35d$ communication. We show in simulations that the communication cost is between $1.35d$ to $1.72d$ on average for all values of d and that it quickly converges to 1.35× when d is in the low hundreds.

(3) An implementation of Rateless IBLT as a library. When reconciling 1000 differences, our implementation can process input data (sets being reconciled) at 120 MB/s using a *single* core of a 2016-model CPU.

(4) Extensive experiments comparing Rateless IBLT with state-of-the-art solutions. Rateless IBLT achieves 3–4× lower communication cost than regular IBLT [12] and MET-IBLT [15], two non-rateless schemes; and 2–2000× lower computation cost than PinSketch [6].

(5) Demonstration of Rateless IBLT's real-world benefits by applying our implementation to synchronize the account states of the Ethereum blockchain. Compared to Merkle trie [38], today's de facto solution, Rateless IBLT achieves 5.6× lower completion time and 4.4× lower communication cost on historic traces.

2 MOTIVATION AND RELATED WORK

We first formally define the set reconciliation problem [7, 19]. Let A and B be two sets containing items (bit strings) of the same length ℓ. A and B are stored by two distinct parties, Alice and Bob. They want to efficiently compute the symmetric difference of A and B, i.e., $(A \cup B) \setminus (A \cap B)$, denoted as $A \triangle B$. By convention [7], we assume that only one of the parties, Bob, wants to compute $A \triangle B$ because he can send the result to Alice afterward if needed.

While straightforward solutions exist, such as exchanging Bloom filters [3] or hashes of the items, they incur $O(|A|+|B|)$ communication and computation costs. The costs can be improved to logarithmic by hashing the sets into Merkle tries [38], where a trie node on depth i is the hash of a $(1/2^i)$-fraction of the set. Alice and Bob traverse and compare their tries, only descending into a sub-trie (subset) if their roots (hashes) differ. However, the costs are still dependent on $|A|$, $|B|$, and now takes $O(\log|A| + \log|B|)$ round trips.

In contrast, the information-theoretic lower bound [19, § 2] of the communication cost is $d\ell$, where $d = |A \triangle B|$.[1] State-of-the-art solutions get close to this lower bound using techniques from coding theory. On a high level, we can view B as a copy of A with d errors (insertions and/or deletions), and the goal of set reconciliation is to correct these errors. Alice *encodes* A into a list of m *coded symbols* and sends them to Bob. Bob then uses the coded symbols and B to decode $A \triangle B$. The coded symbols are the parity data in a systematic error-correcting code that can correct set insertions and deletions [21]. Using appropriate codes, it takes $m = O(d)$ coded symbols, each of length $O(\ell)$, to correct the d errors, resulting in a communication cost of $O(d\ell)$.

The performance of existing solutions varies depending on the codes they use. Characteristic Polynomial Interpolation (CPI) [19] uses a variant of Reed-Solomon codes [28], where coded symbols are evaluations of a polynomial uniquely constructed from A. CPI has a communication cost of $d\ell$, achieving the information-theoretic lower bound. However, its computation cost is $O(|A|d\ell)$ for Alice, and $O(|B|d\ell+d^3\ell^4)$ for Bob. The latter was improved to $O(|B|d\ell + d^2\ell^2)$ in PinSketch [6, 37] using BCH codes [4] that are easier to decode. Nevertheless, as we show in § 7.2, computation on both Alice and Bob quickly becomes intractable even at moderate $|A|$, $|B|$, and d, limiting its applicability. For example, Shrec [13] attempted to use PinSketch to synchronize transactions in a high-throughput blockchain but found that its high computation complexity severely limits system throughput [13, § 5.2].

Invertible Bloom Lookup Tables (IBLTs) [12] use sparse graph codes similar to LT [17] and LDPC [8] codes. Each set item is summed into k coded symbols, denoted as its neighbors in a random, sparse graph. Some variants also consider graphs with richer structures such as varying k depending on the set item [14]. The computation cost is $O(|A|k\ell)$ for Alice, and $O((|B| + d)k\ell)$ for Bob. The communication cost is $O(d\ell)$ with a coefficient strictly larger than 1 (e.g., 4–10 for small d, see § 7.1). Due to their random nature, IBLTs may fail to decode even if properly parameterized [7]. We provide more background on IBLTs in § 3.

The aforementioned discussions assume that the codes are properly *parameterized*. In particular, we need to decide m, the number of coded symbols Alice sends to Bob. Decoding will fail if m is too small compared to d, and we incur redundant communication and computation if m is too large. The optimal choice of m is thus a function of d. However, accurate prediction of d is usually difficult [13, 23], and sometimes outright impossible [25]. Existing systems often resort to online estimation protocols [7] and over-provision m to accommodate the ensuing errors [7, 25].

The case for rateless reconciliation. A key feature of Rateless IBLT is that it can generate an infinite stream of coded symbols for a set, resembling rateless error-correcting codes [5]. For any $m > 0$, the first m coded symbols can reconcile $O(m)$ set differences with a coefficient close to 1 (0.74 in most cases, see § 7.1). This means that Rateless IBLT does not require parameterization, making real-world deployments

[1] More precisely, the lower bound is $d\ell - d\log_2 d$ [19, § 2], but the second term can be neglected when $d \ll 2^\ell$.

easy and robust. Alice simply keeps sending coded symbols to Bob, and Bob can decode as soon as he receives enough—which we show analytically (§ 5) and experimentally (§ 7.1) to be about $1.35d$ in most cases—coded symbols. Neither Alice nor Bob needs to know d beforehand. The encoding and the decoding algorithms have zero parameters.

The concept of incrementally generating coded symbols is first mentioned in CPI [19]. However, as mentioned before, its real-world use has been limited due to the high computation cost. We discuss these limitations in § 7, and demonstrate that Rateless IBLT reduces the computation cost by 2–2000×, while incurring a communication cost of less than 2× the information-theoretic lower bound. Concurrently with our work, MET-IBLT [15] proposes to simultaneously optimize the parameters of IBLTs for multiple pre-selected values of d, e.g., $d_1, d_2, \ldots, d_n$, such that a list of coded symbols for d_i is a prefix/suffix of that for d_j. However, it only considers a few values of d due to the complexity of the optimization so still requires workload-dependent parameterization. As we show in § 7.1, its communication cost is 4–10× higher for the d values that are not optimized for. In addition, MET-IBLT does not provide a practical algorithm to incrementally generate coded symbols. Rateless IBLT does not have any of these issues.

Rateless IBLT offers additional benefits. Imagine that Alice has the canonical system state, and multiple peers wish to reconcile their states with Alice. In a non-rateless scheme, Alice must separately produce coded symbols for each peer depending on the particular number of differences d. This incurs additional computation and storage I/Os for every peer she reconciles with. And, more importantly, Alice must produce the coded symbols on the fly because she does not know d before a peer arrives. In comparison, using Rateless IBLT, Alice simply maintains a universal sequence of coded symbols and streams it to anyone who wishes to reconcile. Rateless IBLT also allows her to incrementally update the coded symbols as she modifies the state (set), further amortizing the encoding costs.

To the best of our knowledge, Rateless IBLT is the first set reconciliation solution that simultaneously achieves the following properties:

- **Ratelessness.** The encoder generates an infinite sequence of coded symbols, capable of reconciling any number of differences d with low overhead.
- **Universality.** The same algorithm works efficiently for any $|A|$, $|B|$, d, and ℓ without any parameter.
- **Low communication cost.** The average communication cost peaks at $1.72d\ell$ when $d = 4$, and quickly converges to $1.35d\ell$ when d is at the low hundreds.
- **Low computation cost.** Encoding costs $O(\ell \log d)$ per set item, and decoding costs $O(\ell \log d)$ per difference. In practice, a single core on a 2016-model CPU can encode (decode) 3.4 million items (differences) per second when $d = 1000$ and $\ell = 8$ bytes.

We demonstrate these advantages by comparing with all the aforementioned schemes in § 7 and applying Rateless IBLT to a potential application in § 7.3.

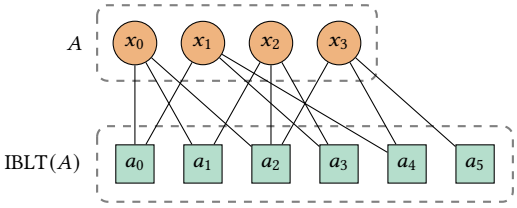

Figure 1: Example of constructing a regular IBLT for set A with source symbols x_0, x_1, x_2, x_3. The IBLT has $m = 6$ coded symbols: $a_0, a_1, a_2, a_3, a_4, a_5$. Each source symbol is mapped to $k = 3$ coded symbols. Solid lines represent the mapping between source and coded symbols. For example, for a_4, `sum` = $x_1 \oplus x_3$, `checksum` = `Hash`(x_1) $\oplus$ `Hash`(x_3), and `count` = 2. $\oplus$ is the bitwise exclusive-or operator.

3 BACKGROUND

Our Rateless IBLT retains the format of coded symbols and the decoding algorithm of regular IBLTs, but employs a new encoder that is oblivious to the number of differences to reconcile. In this section, we provide the necessary background on IBLTs [7, 12] and explain why regular IBLTs fail to provide the rateless property that we desire. We discuss the new rateless encoder in the next section.

On a high level, an IBLT is an encoding of a set. We call the items (bit strings) in the set the *source symbols*, and an IBLT comprises a list of m *coded symbols*. Each source symbol is *mapped* to k coded symbols uniformly at random, e.g., by using k hash functions. Here, m and k are design parameters.

Coded symbol format. A coded symbol contains two fields: `sum`, the bitwise exclusive-or (XOR) sum of the source symbols mapped to it; and `checksum`, the bitwise XOR sum of the hashes of the source symbols mapped to it. In practice, there is usually a third field, `count`, which we will discuss shortly. Fig. 1 provides an example.

Peeling decoder. To recover source symbols from a list of coded symbols, the decoder runs a recursive procedure called "peeling". We say a coded symbol is *pure* when exactly one source symbol is mapped to it; or, equivalently, when its `checksum` equals the hash of its `sum` [7].[2] In this case, its `sum` field is the source symbol itself, which is now recovered. The decoder then removes the recovered source symbol from any other coded symbols it is mapped to (determined by the k agreed-upon hash functions), by XOR-ing the source symbol and its hash into their `sum` and `checksum` fields, respectively.

[2]Unless there is a hash collision, which happens with negligible probability in the length of the hash. See § 4.3.

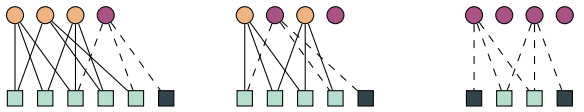

(a) Iteration 1 (b) Iteration 2 (c) Iteration 3

Figure 2: Example of decoding the IBLT in Fig. 1 using peeling. Dark colors represent pure coded symbols at the beginning of each iteration, and source symbols recovered so far. Dashed edges are removed at the end of each iteration, by XOR-ing the source symbol (now recovered) and its hash on one end of the edge into the `sum` and `checksum` fields of the coded symbol on the other end.

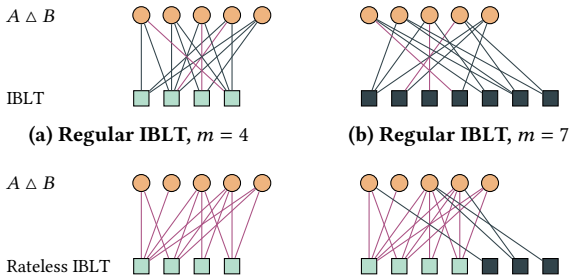

(a) Regular IBLT, $m = 4$ (b) Regular IBLT, $m = 7$

(c) Rateless IBLT, prefix of $m = 4$ (d) Rateless IBLT, prefix of $m = 7$

Figure 3: Regular IBLTs and prefixes of Rateless IBLT for 5 source symbols. Figs. a, c (left) have too few coded symbols and are undecodable. Figs. b, d (right) are decodable. Red edges are common across each row. Dark coded symbols in Figs. b, d are new or changed compared to their counterparts in Figs. a, c. Imagine that Alice sends 4 coded symbols but Bob fails to decode. In regular IBLT, in order to enlarge m, she has to send all 7 coded symbols since the existing 4 symbols also changed. In Rateless IBLT, she only needs to send the 3 new symbols. The existing 4 symbols stay the same.

This process may generate additional pure symbols; the decoder repeats until no pure symbols are left. Decoding fails if it stops before recovering all source symbols [12]. Fig. 2 shows the example of decoding the IBLT in Fig. 1.

Subtraction of coded symbols. $a \oplus b$ denotes subtraction of two coded symbols a, b. For the resulting coded symbol, its `sum` is the bitwise XOR of a.`sum` and b.`sum`; its `checksum` is the bitwise XOR of a.`checksum` and b.`checksum`; and its `count` is a.`count` $- b$.`count`.

Set reconciliation using IBLTs. IBLTs with the same parameter configuration (m, k, and hash functions mapping from source symbols to coded symbols) can be subtracted [7]. For any two sets A and B, $\text{IBLT}(A) \oplus \text{IBLT}(B) = \text{IBLT}(A \triangle B)$, where the $\oplus$ operator subtracts each corresponding pair of coded symbols from the two IBLTs. This is because if a source symbol is present in both A and B, then it is XOR-ed twice into each coded symbol it is mapped to in $\text{IBLT}(A) \oplus \text{IBLT}(B)$, resulting in no effect. As a result, $\text{IBLT}(A) \oplus \text{IBLT}(B)$ is an encoding of the source symbols that appear exactly once across A and B, i.e., $A \triangle B$.

To reconcile A and B, Alice sends $\text{IBLT}(A)$ to Bob, who then computes and decodes $\text{IBLT}(A) \oplus \text{IBLT}(B)$ to recover $A \triangle B$. To determine whether a recovered source symbol belongs to A or B, we use the `count` field.[3] It records the number of source symbols mapped to a coded symbol. When a coded symbol is pure, `count` $= 1$ indicates that the recovered source symbol is exclusive to A, and `count` $= -1$ indicates B [7].

Limitations of IBLTs. IBLTs are not rateless. An IBLT with a particular set of parameters m, k only works for a narrow range of difference size d. It quickly becomes inefficient to use it for more or fewer differences than parameterized for. In Appendix A, we show Theorems A.1 and A.2, which we summarize informally here. First, with high probability, Bob cannot recover *any* source symbol in $A \triangle B$ when $d > m$, making undersized IBLTs completely useless. On the other hand, we cannot simply default to a very large m to accommodate a potentially large d. If d turns out to be small, i.e., $d \ll m$, Alice still has to send almost the entire IBLT (m coded symbols) for Bob to decode successfully, leading to high communication cost. Alice cannot dynamically enlarge m, either. Each source symbol is already uniformly mapped to k out of m coded symbols upon encoding. Increasing m post hoc would require remapping the source symbols to the expanded space of coded symbols so that the mapping remains uniform. This requires Alice to rebuild and re-send the entire IBLT. Figs. 3a, 3b show an example.

[3]Alternatively, Bob may try looking up each item in $A \triangle B$ against B, but this requires indexing B, which is undesirable when $|B|$ is large.

4 DESIGN

For any set S, Rateless IBLT defines an infinite sequence of coded symbols. Intuitively, an infinite number of coded symbols for A and B allows Rateless IBLT to accommodate an arbitrarily large set difference. Every *prefix* of this infinite sequence functions like a normal IBLT and can reconcile a number of differences proportional to its length. Meanwhile, because these prefixes belong to a common infinite sequence, Alice simply streams the sequence until Bob receives a long enough prefix to decode. For any $d > 0$, on average, reconciling d differences requires only the first $1.35d$–$1.72d$ coded symbols in the sequence.

4.1 Coded Symbol Sequence

Our main task is to design the algorithm that encodes any set S into an infinite sequence of coded symbols, denoted as $s_0, s_1, s_2, \ldots$. It should provide the following properties:

- **Decodability.** With high probability, the peeling decoder can recover all source symbols in a set S using a prefix of $s_0, s_1, s_2, \ldots$ with length $O(|S|)$.
- **Linearity.** For any sets A and B, $a_0 \oplus b_0, a_1 \oplus b_1, a_2 \oplus b_2, \ldots$ is the coded symbol sequence for $A \triangle B$.
- **Universality.** The encoding algorithm does not need any extra information other than the set being encoded.

These properties allow us to build the following simple protocol for rateless reconciliation. To reconcile A and B, Alice incrementally sends $a_0, a_1, a_2, \ldots$ to Bob. Bob computes $a_0 \oplus b_0, a_1 \oplus b_1, a_2 \oplus b_2, \ldots$, and tries to decode these symbols using the peeling decoder. Bob notifies Alice to stop when he has recovered all source symbols in $A \triangle B$. As we will soon show, the first symbol $a_0 \oplus b_0$ in Rateless IBLT is decoded only after all source symbols are recovered. This is the indicator for Bob to terminate.

Linearity guarantees that $a_0 \oplus b_0, a_1 \oplus b_1, a_2 \oplus b_2, \ldots$ is the coded symbol sequence for $A \triangle B$. Decodability guarantees that Bob can decode after receiving $O(|A \triangle B|)$ coded symbols and recover all source symbols in $A \triangle B$. Universality guarantees that Alice and Bob do not need any prior context to run the protocol.

If Alice regularly reconciles with multiple peers, she may cache coded symbols for A to avoid recomputing them every session. Universality implies that Alice can reuse the same cached symbols across different peers. Linearity implies that if she updates her set A, she can incrementally update the cached symbols by treating the updates $A \triangle A'$ as a set and subtracting its coded symbols from the cached ones for A.

We now discuss how we design an encoding algorithm that satisfies the three properties we set to achieve.

4.1.1 Linearity & Universality. Our key observation is that to ensure linearity, it is sufficient to define a consistent *mapping rule*, which, given any source symbol $x \in \{0,1\}^*$ and any index $i \geq 0$, deterministically decides whether x should be mapped to the i-th coded symbol when encoding a set that contains x. This ensures that if $x \in A \cap B$, then it will be mapped to both a_i and b_i or neither; in either case, x will not be reflected in $a_i \oplus b_i$. On the other hand, if $x \in A \triangle B$, and x should be mapped to index i according to the rule, then it will be mapped to *exactly* one of a_i or b_i, and therefore will be reflected in $a_i \oplus b_i$. Since the mapping rule makes decisions based only on x and i, the resulting encoding algorithm also satisfies universality.

4.1.2 Decodability. Whether the peeling decoder can recover all source symbols from a set of coded symbols is fully determined by the mapping between the source and the coded symbols. Let $\rho(i)$ be the probability that a random source symbol maps to the i-th coded symbol, which we refer to as the *mapping probability*. It is the key property that defines the behavior of a mapping rule. In the remainder of this subsection, we constrain $\rho(i)$ by examining two necessary conditions for peeling to succeed. Our key conclusion is that in order for decodability to hold, $\rho(i)$ must be inversely proportional to i. This rejects most functions as candidates of $\rho(i)$ and leads us to a concrete instantiation of $\rho(i)$. We will design a concrete algorithm (mapping rule) that realizes the mapping probability in the next subsection, and mathematically prove that it satisfies decodability in § 5.

First, to kick-start the peeling decoder, there must be a coded symbol with exactly one source symbol mapped to it (a pure coded symbol). For a set S and index i, the probability that this happens decreases quasi-exponentially in $\rho(i)|S|$. This implies that $\rho(i)$ must decrease quickly with i. Otherwise, each of the first $O(|S|)$ coded symbols would have an exponentially small probability of being pure, and it would be likely that none of them is pure, violating decodability.

The following lemma shows that for this reason, the mapping probability $\rho(i)$ cannot decrease slower than $1/i^{1-\epsilon}$ for any positive ϵ, i.e., *almost* inversely proportional to i. We defer the proof to Appendix C.

Lemma 4.1. *For any $\epsilon > 0$, any mapping probability $\rho(i)$ such that $\rho(i) = \Omega\left(1/i^{1-\epsilon}\right)$, and any $\sigma > 0$, if there exists at least one pure coded symbol within the first m coded symbols for a random set S with probability σ, then $m = \omega(|S|)$.*

Second, to recover all source symbols in a set S, we need at least $|S|$ non-empty coded symbols. This is because during peeling, each pure symbol (which must be non-empty) yields at most one source symbol. Intuitively, $\rho(i)$ cannot decrease too fast with index i. Otherwise, the probability that a coded symbol is empty would quickly grow towards 1 as i increases. The first $O(|S|)$ coded symbols would not reliably contain at least $|S|$ non-empty symbols, violating decodability.

The following lemma shows that for this reason, the mapping probability $\rho(i)$ cannot decrease faster than $1/i$. We defer the proof to Appendix C.

Lemma 4.2. *For any mapping probability $\rho(i)$ such that $\rho(i) = o(1/i)$, and any $\sigma > 0$, if there exist at least $|S|$ non-empty coded symbols within the first m coded symbols for a random set S with probability σ, then $m = \omega(|S|)$.*

The constraints above reject functions that decrease faster than $1/i$, as well as functions that decrease slower than i^ϵ/i for any $\epsilon > 0$. For simplicity, we ignore the degree of freedom stemming from the i^ϵ factor since for a sufficiently small ϵ and any practical i, it is very close to 1. The remaining candidates for $\rho(i)$ are the ones in between, i.e., functions of order $1/i$. We choose the simplest function in this class:

$$\rho(i) = \frac{1}{1+\alpha i}, \tag{1}$$

where $\alpha > 0$ is a parameter. We shift the denominator by 1 because i starts at 0. In § 5, we prove that this $\rho(i)$ achieves decodability with high efficiency: recovering a set S only requires the first $1.35|S|-1.72|S|$ coded symbols on average.

We highlight two interesting properties of our $\rho(i)$. First, $\rho(0) = 1$. This means that for any set, every source symbol is mapped to the first coded symbol. This coded symbol is only decoded after all source symbols are recovered. So, Bob can tell whether reconciliation has finished by checking if $a_0 \oplus b_0$ is decoded. Second, among the first m indices, a source symbol is mapped to $\sum_{i=0}^{m-1} \rho(i)$ of them on average, or $O(\log m)$. It means that the *density* of the mapping, which decides the computation cost of encoding and decoding, decreases quickly as m increases. As we will show in § 7.2, the low density allows Rateless IBLT to achieve 2–2000× higher throughput than PinSketch.

4.2 Realizing the Mapping Probability

We now design an efficient deterministic algorithm for mapping a source symbol s to coded symbols that achieves the mapping probability rule identified in the previous section.

Recall that for a random source symbol s, we want to make the probability that s is mapped to the i-th coded symbol to be $\rho(i)$ in Eq. 1. A simple strawperson solution, for example, is to use a hash function that, given s, outputs a hash value uniformly distributed in $[0, 1)$. We then compare the hash value to $\rho(i)$, and decide to map s to the i-th coded symbol if the hash value is smaller. Given a random s, because its hash value distributes uniformly, the mapping happens with probability $\rho(i)$.

However, this approach has major issues. First, it requires comparing hash values and $\rho(i)$ for every pair of source symbol s and index i. As mentioned in § 4.1.2, the density of the mapping is $O(\log m)$ for the first m coded symbols. In contrast, generating the m coded symbols using this algorithm would require m comparisons for each source symbol, significantly inflating the computation cost. Another issue is that we cannot use the same hash function when mapping s to different indices i and j. Otherwise, the mappings to them would not be independent: if $\rho(i) < \rho(j)$ and s is mapped to i, then it will always be mapped to j. Using different, independent hash functions when mapping the same source symbol to different indices means that we also need to hash the symbol m times.

We design an algorithm that maps each source symbol to the first m coded symbols using only $O(\log m)$ computation. The strawperson solution is inefficient because we roll a dice (compare hash and $\rho(i)$) for every index i, even though we end up not mapping s to the majority of them ($m - O(\log m)$ out of m), so reaching the next *mapped* index takes many dice rolls ($m/O(\log m)$ on average). Our key idea is to directly sample the distance (number of indices) to *skip* before reaching the next mapped index. We achieve it with constant cost per sample, so we can jump from one mapped index straight to the next in constant time.

We describe our algorithm recursively. Suppose that, according to our algorithm, a source symbol s has been mapped to the i-th coded symbol. We now wish to compute, in constant time, the *next* index j that s is mapped to. Let G be the random variable such that $j - i = G$ for a random s, and let P_g ($g \geq 1$) be the probability that $G = g$. In other words, P_g is the probability that a random s is not mapped to any of $i+1, i+2, \ldots, i+g-1$, but is mapped to $i+g$, which are all independent events. So,

$$P_g = (1-\rho(i+1))(1-\rho(i+2))\ldots(1-\rho(i+g-1))\rho(i+g).$$

Generating j is then equivalent to sampling $g \leftarrow G$, whose distribution is described by P_g, and then computing $j = i + g$.

However, since there are g (which can go to infinity) terms in P_g, it is still unclear how to sample G in constant time. The key observation is that when we set the parameter $\alpha = 0.5$ in $\rho(i)$, most of the terms in P_g cancel out, and

$$P_g = \frac{2(i+1)(i+2)}{(i+g)(i+g+1)(i+g+2)}.$$

Let $C(x)$ be the cumulative mass function of G. It also has a remarkably simple form

$$C(x) = \sum_{g=1}^{x} P_g = \frac{x(2i+x+3)}{(i+x+1)(i+x+2)}.$$

We defer the step-by-step derivation of P_g and $C(x)$ to Appendix B.

Let $C^{-1}(r)$ be the inverse of $C(x)$,

$$C^{-1}(r) = \sqrt{\frac{(3+2i)^2 - r}{4(1-r)}} - \frac{3+2i}{2}.$$

In practice, we use the following approximation,

$$C^{-1}(r) \approx (1.5+i)((1-r)^{-\frac{1}{2}} - 1).$$

To sample G, we sample $r \leftarrow [0, 1)$ uniformly, and compute $g = \lceil C^{-1}(r) \rceil$. To make the algorithm deterministic, r may come from a pseudorandom number generator seeded with the source symbol s. The algorithm outputs $i + g$ as the next index to which s is mapped, updates $i \leftarrow i + g$, and is ready to produce another index. Because every source symbol is mapped to the first coded symbol (recall that $\rho(0) = 1$), we start the recursion with $i = 0$.

4.3 Resistance to Malicious Workload

In some distributed applications, a node may reconcile its state against multiple peers who are supposed to hold replicas of the system state. The common motivation is fault

tolerance, where one node may go offline, forcing the recipient to receive updates from another; censorship resistance, where the recipient wants to make sure no peer hides information (e.g., social media posts from Alice, or her blockchain transactions); and efficiency, since updating simultaneously from multiple peers may be faster than choosing just one source.

In some applications, rogue users may inject items to Alice or Bob's sets. For example, in a distributed social media application where servers exchange posts, users can craft any post they like. This setting may create an "adversarial workload," where the hash of the symbol representing the user's input does not distribute uniformly. If the user injects into Bob's set a source symbol that hashes to the same value as another source symbol that Alice has, then Bob will never be able to reconcile its set with Alice. This is because Bob will XOR the malicious symbol into the coded symbol stream it receives from Alice, but it will only cancel out the hash of Alice's colliding symbol from the `checksum` field, and will corrupt the `sum` field.

The literature on set reconciliation is aware of this issue, but typically does not specify the required properties from the hash function to mitigate it, or assumes strong properties such as random oracles [20], which have long outputs (say, 256 bits). It is sufficient, however, to use a keyed hash function with uniform and shorter outputs (say, 64 bits). This allows Alice and Bob to coordinate a secret key and use it to choose a hash function from the family of keyed hashes. Although with short hash images, an attacker can computationally enumerate enough symbols to find a collision for an item that Alice has, the attacker does not know the key, i.e., the hash function that Alice and Bob use, so she cannot target a collision to one of Alice's symbols. This allows Rateless IBLT to minimize the size of a coded symbol and save bandwidth, particularly in applications where symbols are short and `checksums` account for much of the overhead. In practice, we use the SipHash [2] keyed hash function. A trade-off we make is that Alice has to compute the `checksums` separately for each key she uses, which increases her computation load. We believe this is a worthwhile trade-off as SipHash is very efficient, and we find in experiments (§ 7.2) that computing the hashes has negligible cost compared computing `sums`, which are still universal. Also, we expect using different keys only in applications where malicious workload is a concern.

5 ANALYSIS

In this section, we use density evolution [18, 29] to analyze the behavior of the peeling decoder for symbols coded with Rateless IBLT. We mathematically prove that as the difference size d goes to infinity, the *overhead* of Rateless IBLT converges to 1.35; i.e., reconciling d differences requires only the first $1.35d$ coded symbols. We then use Monte Carlo simulations to show that the convergence happens quickly, when d is at the low hundreds.

Density evolution is a standard technique for analyzing the iterative decoding processes in error correcting codes [18, 29], and has been applied to IBLTs with simpler mappings between source and coded symbols [14]. Its high-level idea is to iteratively compute the probability that a random source symbol has *not* been recovered while simulating the peeling decoder statistically. If this probability keeps decreasing towards 0 as the peeling decoder runs for more iterations, then decoding will succeed with probability converging to 1 [18, § 2]. The following theorem states our main conclusion. In the interest of space, we defer its proof to Appendix C.

Theorem 5.1. *For a random set of n source symbols, the probability that the peeling decoder successfully recovers the set using the first ηn coded symbols (as defined in § 4) tends to 1 as n goes to infinity, provided that η is any positive constant such that*

$$\forall q \in (0, 1] : e^{\frac{1}{\alpha} Ei\left(-\frac{q}{\alpha\eta}\right)} < q. \tag{2}$$

Recall that $\mathrm{Ei}(\cdot)$ is the exponential integral function[4]; α is the parameter in $\rho(i) = \frac{1}{1+\alpha i}$ as discussed in § 4. We stated Theorem 5.1 with respect to a generic set of source symbols and its corresponding coded symbol sequence; in practice, the set is $A \triangle B$. The decoder (Bob) knows the coded symbol sequence for $A \triangle B$ because he subtracts the coded symbols for B (generated locally) from those for A (received from Alice) as defined in § 3.

Theorem 5.1 implies that there exists a threshold η^*, which is the smallest η that satisfies Eq. 2. Any $\eta > \eta^*$ also satisfies Eq. 2 because the left-hand side strictly decreases with respect to η. As long as Bob receives more than η^* coded symbols per source symbol, he can decode with high probability. In other words, η^* is the communication *overhead* of Rateless IBLT, i.e., the average number of coded symbols required to recover each source symbol. Recall that we set $\alpha = 0.5$ in our final design as discussed in § 4.2. We solve for η^* and get the following result.

Corollary 5.2. *The average overhead of Rateless IBLT converges to* 1.35 *as the difference size $d = |A \triangle B|$ goes to infinity.*

In the appendix, we explore how α affects η^* (see Fig. 14) and confirm that setting $\alpha = 0.5$ is close to optimal.

Theorem 5.1 and Corollary 5.2 from density evolution state the behavior of Rateless IBLT when the difference size d goes to infinity. To understand the behavior when d is finite, we run Monte Carlo simulations, and compare the results with the theorems. Fig. 4 shows the overhead at different d. It peaks at 1.72 when $d = 4$ and then converges to 1.35, as

[4] $\mathrm{Ei}(x) = -\int_{-x}^{\infty} \frac{e^{-t}dt}{t}$.

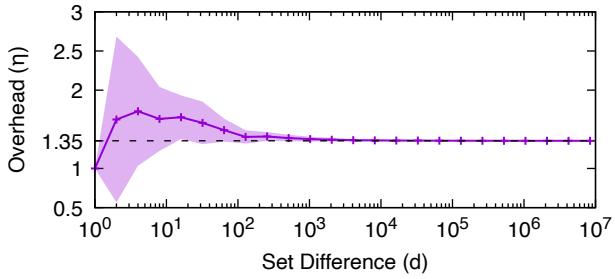

Figure 4: Overhead of Rateless IBLT at varying difference sizes d. We run 100 simulations for each data point. The shaded area shows the standard deviation. The dashed line shows 1.35, the overhead predicted by density evolution.

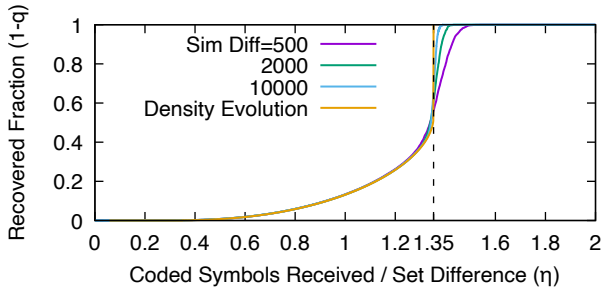

Figure 5: The fraction of recovered source symbols after receiving different number of coded symbols (normalized over the difference size d), as observed in simulations (1000 times), and as predicted by density evolution. Dashed line shows 1.35, the overhead predicted by density evolution.

predicted by Corollary 5.2. Convergence happens quickly: for all $d > 128$, the overhead is less than 1.40.

The fixed points of q in Eq. 2 represent the expected fraction of source symbols that the peeling decoder fails to recover before stalling, as d goes to infinity. Fig. 5 compares this result with simulations (we plot $1 - q$, the fraction that the decoder *can* recover). The result matches closely to simulations. There is a sharp increase in the fraction of recovered source symbols towards the end, a behavior also seen in other codes that use the peeling decoder, such as LT codes [17].

6 IMPLEMENTATION

We implement Rateless IBLT as a library in 353 lines of Go code. The implementation is self-contained and does not use third-party code. In this section, we discuss some important optimizations in the implementation.

Efficient incremental encoding. A key feature of Rateless IBLT is that it allows Alice to generate and send coded symbols one by one until Bob can decode. Suppose that Alice has generated coded symbols until index $i - 1$, and now wishes to generate the i-th coded symbol. She needs to quickly find the source symbols that are mapped to it. A strawperson solution is to store alongside each source symbol the next index it is mapped to, and scan all the source symbols to find the ones mapped to i. However, this takes $O(|A|)$ time. In our implementation, we store pointers to source symbols in a *heap*. It implements a priority queue, where the priority is the index of the next coded symbol that a source symbol is mapped to. A smaller value indicates higher priority. This ensures that source symbols used for generating the next coded symbol are always at the head of the queue so that the encoder can access them efficiently without scanning all the source symbols.

Variable-length encoding for `count`. Recall that the `count` field stores the number of source symbols that are mapped to a coded symbol during encoding. The standard approach is to allocate a fixed number of bytes for it [7, 15], which inflates the size of each coded symbol by a constant amount. However, in Rateless IBLT, the value stored in `count` decreases with the index of the coded symbol according to a known pattern: the i-th coded symbol for a set S is expected to have a `count` of $|S|\rho(i)$. This pattern allows us to aggressively compress the `count` field. Instead of storing the value itself, we can store the *difference* of the actual value and the aforementioned expected value, which is a much smaller number. The node receiving the coded symbol can reconstruct the actual value of `count`, because it knows N (transmitted with the 0-th coded symbol) and i (assuming a transport that preserves ordering). Instead of allocating a fixed number of bytes, we use variable-length quantity [35] to store the difference, which uses $\lceil \log_{128} x \rceil$ bytes to store any number x. Using our approach, the `count` field takes only 1.05 bytes per coded symbol on average when encoding a set of 10^6 items into 10^4 coded symbols, keeping the resulting communication cost to a minimum.

7 EVALUATION

We compare Rateless IBLT with state-of-the-art set reconciliation schemes, and demonstrate its low communication (§ 7.1) and computation (§ 7.2) costs across a wide range of workloads (set sizes, difference sizes, and item lengths). We then apply Rateless IBLT to synchronize the account states of Ethereum and demonstrate significant improvements over the production system on real workloads (§ 7.3).

Schemes compared. We compare with regular IBLT [7, 12], MET-IBLT [15], PinSketch [6], and Merkle tries [38]. For Rateless IBLT, we use our implementation discussed in § 6. For regular IBLT and MET-IBLT, we implement each scheme in Python. We use the recommended parameters [7, § 6.1][15, §§ V-A, V-C], and allocate 8 bytes for the `checksum` and the `count` fields, respectively. For PinSketch, we use Minisketch [23, § 6], a state-of-the-art implementation [37] written in C++ and deployed in Bitcoin. For Merkle tries, we

use the implementation in Geth [9], the most popular client for Ethereum.

7.1 Communication Cost

We first measure the communication *overhead*, defined as the amount of data transmitted during reconciliation divided by the size of set difference accounted in bytes. We test with set differences of 1–400 items. Beyond 400, the overhead of all schemes stays stable. The set size is 1 million items (recall that it only affects Merkle trie's communication cost). Each item is 32 bytes, the size of a SHA256 hash, commonly used as keys in open-permission distributed systems [22, 34]. For Rateless IBLT and MET-IBLT, we generate coded symbols until decoding succeeds, repeat each experiment 100 times, and then report the average overhead and the standard deviation. Regular IBLTs cannot be dynamically expanded, and tuning the number of coded symbols m requires precise knowledge of the size of the set difference. Usually, this is achieved by sending an estimator before reconciliation [7], which incurs an extra communication cost of at least 15 KB according to the recommended setup [15, § V-C]. We report the overhead of regular IBLT with and without this extra cost. Also, unlike the other schemes, regular IBLTs may fail to decode probabilistically. We gradually increase the number of coded symbols m until the decoding failure rate drops below 1/3 000.

Fig. 6 shows the overhead of all schemes except for Merkle trie, whose overhead is significantly higher than the rest at over 40 across all difference sizes we test. Rateless IBLT consistently achieves lower overhead compared to regular IBLT and MET-IBLT, especially when the set difference is small. For example, the overhead is 3–4× lower when the set difference is less than 50. The improvement is more significant when considering the cost of the estimator for regular IBLTs. On the other hand, PinSketch consistently achieves an overhead of 1, which is 37–60% lower than Rateless IBLT. However, as we will soon show, Rateless IBLT incurs 2–2 000× less computation than PinSketch on both the encoder and the decoder. We believe that the extra communication cost is worthwhile in most applications for the significant reduction in computation cost.

Scalability of Rateless IBLT. We quickly remark on how Rateless IBLT's communication cost scales to longer or shorter items. Like other schemes based on sparse graphs, the `checksum` and `count` fields add a constant cost to each coded symbol. For Rateless IBLT, these two fields together occupy about 9 bytes. Longer items will better amortize this fixed cost. When reconciling shorter items, this fixed cost might become more prominent. However, it is possible to reduce the length of the `checksum` field if the differences are smaller, because there will be fewer opportunities for hash collisions. We found that hashes of 4 bytes are enough to reliably reconcile differences of tens of thousands. It is also possible to remove the `count` field altogether; Bob can still recover the symmetric difference as the peeling decoder (§ 3) does not use this field.

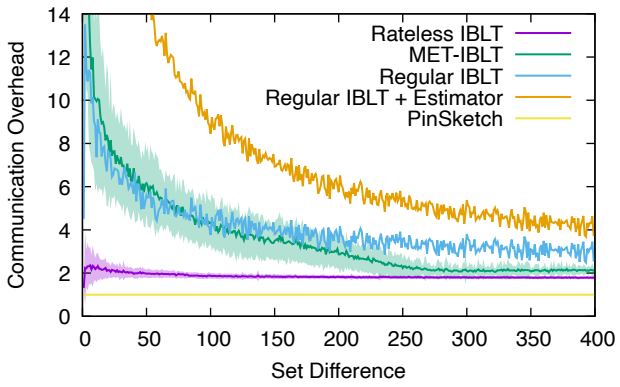

Figure 6: Communication overhead of various schemes. Each item is 32 bytes. Shaded areas show the standard deviation for Rateless IBLT and MET-IBLT. Regular IBLT + Estimator shows the overhead of regular IBLT with an estimator for the size of set difference. We do not plot for Merkle Trie as its overhead is significantly higher (over 40) than the rest.

7.2 Computation Cost

There are two potential computation bottlenecks in set reconciliation: encoding the sets into coded symbols, and decoding the coded symbols to recover the symmetric difference. Encoding happens at Alice, and both encoding and decoding happen at Bob. In this experiment, we measure the encoding and decoding throughput for sets of various sizes and differences. We focus on comparing with PinSketch. We fix the item size to 8 bytes, because this is the maximum size that the PinSketch implementation supports. We do not compare with regular IBLT or MET-IBLT as we cannot find high-quality open source implementations, and they have similar complexity as Rateless IBLT.[5] We will compare with Merkle trie in § 7.3. We run the benchmarks on a server with two Intel Xeon E5-2697 v4 CPUs. Both Rateless IBLT and PinSketch are single-threaded, and we pin the executions to one CPU core using `cpuset(1)`.

Encoding. Fig. 7 shows in solid lines the encoding throughput, defined as the difference size divided by the time it takes for the encoder to generate enough coded symbols for successful reconciliation. It indicates the number of items that

[5]The complexity is linear to the average number of coded symbols each source symbol is mapped to.This is $O(\log(m))$ for Rateless IBLT and MET-IBLT [15], and constant for regular IBLT, where m is the number of coded symbols. However, the cost is amortized over the size of the set difference, which is $O(m)$. So, in all three IBLT-based schemes, the cost to encode for *each* set difference decreases quickly as m increases.

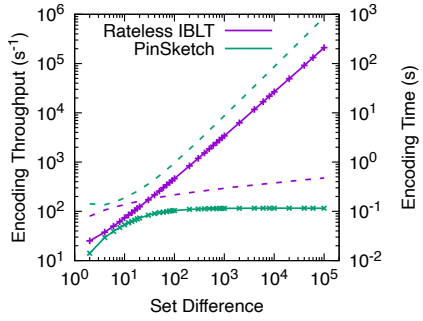

(a) $N = 1\,000\,000$

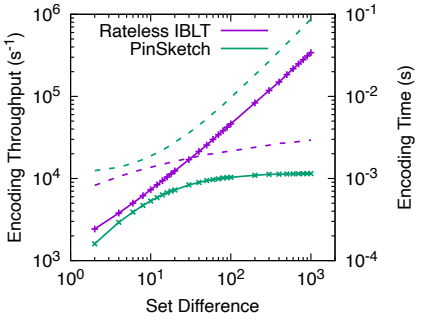

(b) $N = 10\,000$

Figure 7: Encoding throughput and time for sets of sizes $N = 1\,000\,000$ and $N = 10\,000$. Solid lines show the throughput (left Y-axis), and dashed lines show the encoding time (right Y-axis).

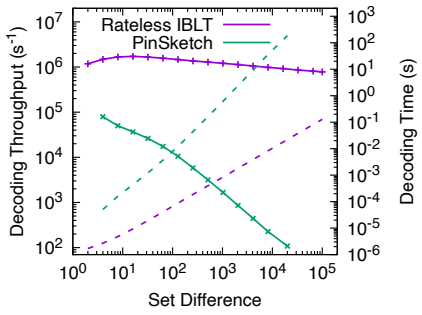

Figure 8: Decoding throughput and time. Solid lines show the throughput (left Y-axis), and dashed lines show the decoding time (right Y-axis).

can be reconciled per second with a compute-bound encoder. Rateless IBLT achieves 2–2000× higher encoding throughput than PinSketch when reconciling differences of 2–10^5 items. The significant gain is because the mapping between source and coded symbols is *sparse* in Rateless IBLT, and the sparsity increases rapidly with m, so the average cost to generate a coded symbol decreases quickly. In comparison, generating a coded symbol in PinSketch always requires evaluating the entire characteristic polynomial, causing the throughput to converge to a constant.

As the difference size increases, the encoding throughput of Rateless IBLT increases *almost* linearly, enabling the encoder to scale to large differences. In Fig. 7, we plot in dashed lines the time it takes to finish encoding. As the difference size increases by 50 000×, the encoding time of Rateless IBLT grows by less than 6×. Meanwhile, the encoding time of PinSketch grows by 5 000×.

Decoding. Fig. 8 shows the decoding throughput (solid lines) and time (dashed lines), defined similarly as in the encoding experiment. We do not make a distinction of the set size, because it does not affect the decoding complexity. (Recall that decoders operate on coded symbols of the symmetric difference only.) Rateless IBLT achieves 10–$10^7\times$ higher decoding throughput than PinSketch. This is because decoding PinSketch is equivalent to interpolating polynomials [6], which has $O(m^2)$ complexity [37], while decoding Rateless IBLT has only $O(m \log(m))$ complexity thanks to the sparse mapping between source and coded symbols. As the difference size grows by 50 000×, the decoding throughput of Rateless IBLT drops by only 34%, allowing it to scale to large differences. For example, it takes Rateless IBLT 0.01 second to decode 10^5 differences. In contrast, it takes PinSketch more than a minute to decode 10^4 differences.

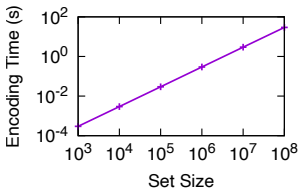

Figure 9: Encoding time of 1 000 differences and varying set size N.

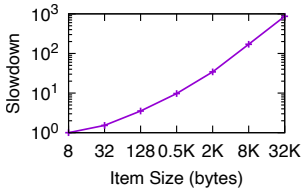

Figure 10: Slowdown when encoding items of different sizes.

Scalability of Rateless IBLT. We now show that Rateless IBLT preserves its computation efficiency when scaling to larger sets, larger differences, and longer items.

The set size N affects encoding, but not decoding, because the decoder operates on coded symbols that represent the symmetric difference. The computation cost of encoding grows linearly with N, as each source symbol is mapped to the same number of coded symbols on average and thus adds the same amount of work. For example, in Fig. 7, the encoding time for 10^3 differences is 2.9 milliseconds when $N = 10^4$, and 294 milliseconds when $N = 10^6$, a difference of 100× that matches the change in N. Fig. 9 shows the encoding time measured in experiments with the same configuration for a wider range of N.

The difference size d affects both encoding and decoding. Recall that Rateless IBLT uses about $1.35d$ coded symbols to reconcile d differences (§ 5). As d increases, the encoder needs to generate more coded symbols. However, unlike PinSketch where the cost is linear in d, the cost of Rateless IBLT grows logarithmically. For example, in Fig. 7a, the encoding time grows by only 6× as the set difference increases from 1 to 10^5. This is because the mapping from source to coded symbols is sparse: each source symbol is only mapped to an average of $O(\log d)$ coded symbols. The same result applies to decoding.

For example, in Fig. 8, the decoding throughput drops by 2× as the d grows by 10^4×.

The item size ℓ affects both encoding and decoding because it decides the time it takes to compute the XOR of two symbols, which dominates the computation cost in Rateless IBLT. Fig. 10 shows the relative slowdown when as ℓ grows from 8 bytes to 32 KB. Initially, the slowdown is sublinear (e.g., less than 4× when ℓ grows by 16× from 8 to 128 bytes) because the other costs that are independent of ℓ (e.g., generating the mappings) are better amortized. However, after 2 KB, the slowdown becomes linear. This implies that the data rate at which the encoder can process source symbols, measured in bytes per second, stays constant. For example, when encoding for $d = 1000$, the encoder can process source symbols at 124.8 MB/s. The same analysis applies to decoding. In comparison, tæhe encoding complexity of PinSketch increases linearly with ℓ, and the decoding complexity increases quadratically [6, 37].

7.3 Application

We now apply Rateless IBLT to a prominent application, the Ethereum blockchain. Whenever a blockchain replica comes online, it must synchronize with others to get the latest *ledger state* before it can validate new transactions or serve user queries. The ledger state is a key-value table, where the keys are 20-byte wallet addresses, and the values are 72-byte account states such as its balance. There are 230 million accounts as of January 4, 2024. Synchronizing the ledger state is equivalent to reconciling the set of all key-value pairs, a natural application of Rateless IBLT.

Ethereum (as well as most other blockchains) currently uses Merkle tries (§ 2) to synchronize ledger states between replicas. It applied a few optimizations: using a 16-ary trie instead of a binary one, and shortening sub-tries that have no branches. The protocol is called *state heal* and has been deployed in Geth [9], the implementation which accounts for 84% of all Ethereum replicas [24]. Variants of Geth also power other major blockchains, such as Binance Smart Chain and Optimism.

State heal retains the issues with Merkle tries despite the optimizations. To discover a differing key-value pair (leaf), replicas must visit and compare every internal node on the branch from the root to the differing leaf. This amplifies the communication, computation, and storage I/O costs by as much as the depth of the trie, i.e., $O(\log(N))$ for a set of N key-value pairs. In addition, replicas must descend the branch in lock steps, so the process takes $O(\log(N))$ round trips. As a result, some Ethereum replicas have reported spending weeks on state heal, e.g., [10]. In comparison, Rateless IBLT does not have these issues. Its communication and computation costs depend only on the size of the difference

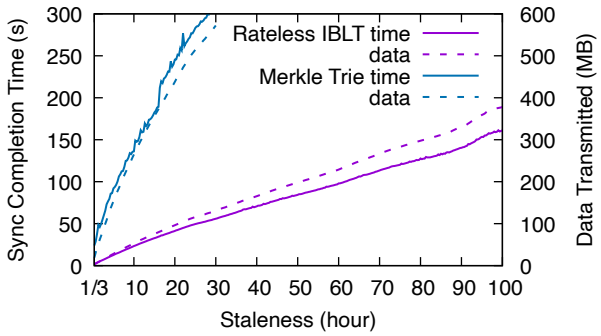

Figure 11: Completion time and communication cost when synchronizing Ethereum ledger states at different staleness over a network link with 50 ms of propagation delay and 20 Mbps of bandwidth. A staleness of x hours means the state is x-hours old when synchronization starts.

rather than the entire ledger state, and it requires no interactivity between replicas besides streaming coded symbols at line rate.

Setup. We compare state heal with Rateless IBLT in synchronizing Ethereum ledger states. We implement a prototype in 1,903 lines of Go code. The prototype is able to load a snapshot of the ledger state from the disk, and synchronize with a peer over the network using either scheme. For state heal, we use the implementation [11] in Geth v1.13.10 without modification. For Rateless IBLT, we use our implementation discussed in § 6. We wrap it with a simple network protocol where a replica requests synchronization by opening a TCP connection to the peer, and the peer streams coded symbols until the requesting replica closes the connection to signal successful decoding.

To obtain workload for experiments, we extract snapshots of Ethereum ledger states as of blocks 18908312–18938312, corresponding to a 100-hour time span between December 31, 2023 and January 4, 2024. Each snapshot represents the ledger state when a block was just produced in the live Ethereum blockchain.[6] For each experiment, we set up two replicas: Alice always loads the latest snapshot (block 18938312); Bob loads snapshots of different staleness and synchronizes with Alice. This simulates the scenario where Bob goes offline at some point in time (depending on the snapshot he loads), wakes up when block 18938312 was just produced, and synchronizes with Alice to get the latest ledger state. We run both replicas on a server with two Intel Xeon E5-2698 v4 CPUs running FreeBSD 14.0. We use Dummynet [30] to inject a 50 ms one-way propagation delay between the replicas and enforce different bandwidth caps of 10 to 100 Mbps.

[6]Ethereum produces a block every 12 seconds. Each block is a batch of transactions that update the ledger state.

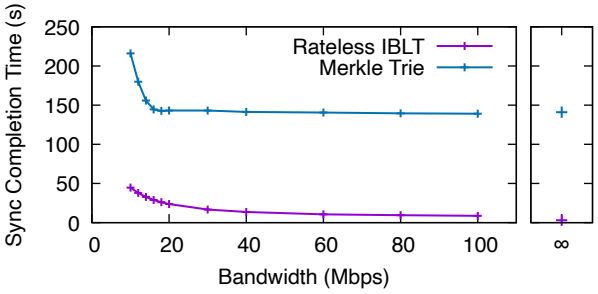

Figure 12: Completion time when synchronizing Ethereum ledger states that are 10 hours stale over a network link with 50 ms of propagation delay and different bandwidth.

Results. We first vary the state snapshot that Bob loads and measure the completion time and the communication cost for Bob to synchronize with Alice. We fix the bandwidth to 20 Mbps. Fig. 11 shows the results. As Bob's state becomes more stale, more updates happen between his and the latest states, and the difference between the two grows linearly. As a result, the completion time and the communication cost of both schemes increase linearly. Meanwhile, Rateless IBLT consistently achieves 5.6–13.6× lower completion time, and 4.4–6.9× lower communication cost compared to state heal. As discussed previously, state heal has a much higher communication cost because it requires transmitting the differing internal nodes of the Merkle trie in addition to the leaves. For example, this amplifies the number of trie nodes transmitted by 3.6× when Bob's state is 30 hours stale. The higher communication cost leads to proportionately longer completion time as the system is throughput-bound. We observe similar gains when Bob loads fresher states, e.g., ones less than 20 minutes stale, as shown in Fig. 15 in Appendix E.

In our experiments, state heal requires at least 11 rounds of interactivity, as Alice and Bob descend from the roots of their tries to the differing leaves in lock steps. Rateless IBLT, in comparison, only requires half of a round because Alice streams coded symbols without waiting for any feedback. This advantage is the most obvious when reconciling a small difference, where the system would be latency-bound. For example, Rateless IBLT is 8.2× faster than state heal when Bob's ledger state is only 1 block (12 seconds) stale. See Fig. 16 in Appendix E for traces of this experiment that highlight the impact of interactivity.

Finally, we demonstrate that Rateless IBLT consistently outperforms state heal across different network conditions. We fix Bob's snapshot to be 10 hours stale and vary the bandwidth cap. Fig. 12 shows the results. Rateless IBLT is 4.8× faster than state heal at 10 Mbps, and the gain increases to 16× at 100 Mbps. Notice that the completion time of state heal stays constant after 20 Mbps; it cannot utilize any extra bandwidth. We observe that state heal becomes *compute-bound*: Bob cannot process the trie nodes he receives fast enough to saturate the network. The completion time does not change even if we remove the bandwidth cap. In contrast, Rateless IBLT is throughput-bound, as its completion time keeps decreasing with the increasing bandwidth. If we remove the bandwidth cap, Rateless IBLT takes 2.5 seconds to finish and can saturate a 170 Mbps link using one CPU core on each side.

Before ending, we quickly discuss a few other potential solutions and how Rateless IBLT compares with them. When Bob's state is consistent with some particular block, he may request Alice to compute and send the state *delta* from his block to the latest block, which would be as efficient as an optimal set reconciliation scheme. However, this is often not the case when Bob needs synchronization, such as when he recovers from database corruption or he has downloaded inconsistent shards of state snapshots from multiple sources, routine when Geth replicas bootstrap [33]. Rateless IBLT (and state heal) does not assume consistent states. Coded symbols in traditional set reconciliation schemes like regular IBLT are tailored to a fixed difference size (§ 3). Alice has to generate a new batch of coded symbols for each peer with a different state. This would add minutes to the latency for large sets like Ethereum, incur significant computation costs, and create denial-of-service vulnerabilities.[7] In contrast, Rateless IBLT allows Alice to prepare a single stream of coded symbols that is efficient for all peers. Because of linearity (§ 4), Alice can incrementally update the coded symbols as her ledger state changes. For an average Ethereum block, it takes 11 ms to update 50 million coded symbols (7 GB) using one CPU core to reflect the state changes.

8 CONCLUSION

We designed, mathematically analyzed, and experimentally evaluated Rateless IBLT. To the best of our knowledge, Rateless IBLT is the first set reconciliation solution with universally low computation cost and near-optimal communication cost across workloads. The distinguishing feature is *ratelessness*: it encodes any set into an infinitely long codeword, of which any prefix is capable of reconciling a proportional number of differences with another set. Ratelessness simplifies deployment as there is no parameter; reduces overhead as nodes can incrementally send longer prefixes without over- or under-committing resources to fixed-sized codewords; and naturally supports concurrent synchronization with multiple nodes. We mathematically proved its asymptotic efficiency and showed that the actual performance converges quickly with extensive simulations. We implemented Rateless IBLT

[7] These issues also apply to the aforementioned state delta solution to a lesser degree, because Alice has to compute the state deltas on the fly.

as a library and benchmarked its performance. Finally, we applied Rateless IBLT to a popular distributed application and demonstrated significant gains in state synchronization over the production system.

ACKNOWLEDGEMENTS

Lei Yang is supported by a gift from the Ethereum Foundation.

REFERENCES

[1] Elli Androulaki, Artem Barger, Vita Bortnikov, Christian Cachin, Konstantinos Christidis, Angelo De Caro, David Enyeart, Christopher Ferris, Gennady Laventman, Yacov Manevich, et al. 2018. Hyperledger fabric: a distributed operating system for permissioned blockchains. In *Proceedings of the thirteenth EuroSys conference*. 1–15.

[2] Jean-Philippe Aumasson and Daniel J Bernstein. 2012. SipHash: a fast short-input PRF. In *International Conference on Cryptology in India*. Springer, 489–508.

[3] Burton H Bloom. 1970. Space/time trade-offs in hash coding with allowable errors. *Commun. ACM* 13, 7 (1970), 422–426.

[4] Raj Chandra Bose and Dwijendra K Ray-Chaudhuri. 1960. On a class of error correcting binary group codes. *Information and control* 3, 1 (1960), 68–79.

[5] John W Byers, Michael Luby, Michael Mitzenmacher, and Ashutosh Rege. 1998. A digital fountain approach to reliable distribution of bulk data. *ACM SIGCOMM Computer Communication Review* 28, 4 (1998), 56–67.

[6] Yevgeniy Dodis, Leonid Reyzin, and Adam Smith. 2004. Fuzzy extractors: How to generate strong keys from biometrics and other noisy data. In *Advances in Cryptology-EUROCRYPT 2004: International Conference on the Theory and Applications of Cryptographic Techniques, Interlaken, Switzerland, May 2-6, 2004. Proceedings 23*. Springer, 523–540.

[7] David Eppstein, Michael T Goodrich, Frank Uyeda, and George Varghese. 2011. What's the difference? Efficient set reconciliation without prior context. *ACM SIGCOMM Computer Communication Review* 41, 4 (2011), 218–229.

[8] Robert Gallager. 1962. Low-density parity-check codes. *IRE Transactions on information theory* 8, 1 (1962), 21–28.

[9] The go-ethereum Authors. 2024. go-ethereum: Official Go implementation of the Ethereum protocol. https://geth.ethereum.org.

[10] The go-ethereum Authors. 2024. State heal phase is very slow (not finished after 2 weeks). https://github.com/ethereum/go-ethereum/issues/23191.

[11] The go-ethereum Authors. 2024. trie package - go-ethereum. https://pkg.go.dev/github.com/ethereum/go-ethereum/trie.

[12] Michael T Goodrich and Michael Mitzenmacher. 2011. Invertible bloom lookup tables. In *2011 49th Annual Allerton Conference on Communication, Control, and Computing (Allerton)*. IEEE, 792–799.

[13] Yilin Han, Chenxing Li, Peilun Li, Ming Wu, Dong Zhou, and Fan Long. 2020. Shrec: Bandwidth-efficient transaction relay in high-throughput blockchain systems. In *Proceedings of the 11th ACM Symposium on Cloud Computing*. 238–252.

[14] Francisco Lázaro and Balázs Matuz. 2021. Irregular invertible Bloom look-up tables. In *2021 11th International Symposium on Topics in Coding (ISTC)*. IEEE, 1–5.

[15] Francisco Lázaro and Balázs Matuz. 2023. A rate-compatible solution to the set reconciliation problem. *IEEE Transactions on Communications* (2023).

[16] Lucien Le Cam. 1960. An approximation theorem for the Poisson binomial distribution. (1960).

[17] Michael Luby. 2002. LT codes. In *The 43rd Annual IEEE Symposium on Foundations of Computer Science, 2002. Proceedings.* IEEE Computer Society, 271–271.

[18] Michael Luby, Michael Mitzenmacher, and Mohammad Amin Shokrollahi. 1998. Analysis of Random Processes via And-Or Tree Evaluation. In *SODA*, Vol. 98. 364–373.

[19] Yaron Minsky, Ari Trachtenberg, and Richard Zippel. 2003. Set reconciliation with nearly optimal communication complexity. *IEEE Transactions on Information Theory* 49, 9 (2003), 2213–2218.

[20] Michael Mitzenmacher and Rasmus Pagh. 2018. Simple multi-party set reconciliation. *Distributed Computing* 31 (2018), 441–453.

[21] Michael Mitzenmacher and George Varghese. 2012. Biff (Bloom filter) codes: Fast error correction for large data sets. In *2012 IEEE International Symposium on Information Theory Proceedings*. IEEE, 483–487.

[22] Satoshi Nakamoto. 2008. Bitcoin: A peer-to-peer electronic cash system. (2008).

[23] Gleb Naumenko, Gregory Maxwell, Pieter Wuille, Alexandra Fedorova, and Ivan Beschastnikh. 2019. Erlay: Efficient transaction relay for bitcoin. In *Proceedings of the 2019 ACM SIGSAC Conference on Computer and Communications Security*. 817–831.

[24] one-three-three seven. 2024. Ethereum Execution Client Diversity. https://execution-diversity.info (retrieved January 22, 2024).

[25] A Pinar Ozisik, Gavin Andresen, Brian N Levine, Darren Tapp, George Bissias, and Sunny Katkuri. 2019. Graphene: efficient interactive set reconciliation applied to blockchain propagation. In *Proceedings of the ACM Special Interest Group on Data Communication*. 303–317.

[26] Neil Perry, Bruce Spang, Saba Eskandarian, and Dan Boneh. 2022. Strong Anonymity for Mesh Messaging. *arXiv preprint arXiv:2207.04145* (2022).

[27] Aravindh Raman, Sagar Joglekar, Emiliano De Cristofaro, Nishanth Sastry, and Gareth Tyson. 2019. Challenges in the decentralised web: The mastodon case. In *Proceedings of the internet measurement conference*. 217–229.

[28] Irving S Reed and Gustave Solomon. 1960. Polynomial codes over certain finite fields. *Journal of the society for industrial and applied mathematics* 8, 2 (1960), 300–304.

[29] Thomas J Richardson and Rüdiger L Urbanke. 2001. The capacity of low-density parity-check codes under message-passing decoding. *IEEE Transactions on information theory* 47, 2 (2001), 599–618.

[30] Luigi Rizzo. 1997. Dummynet: a simple approach to the evaluation of network protocols. *ACM SIGCOMM Computer Communication Review* 27, 1 (1997), 31–41.

[31] J Michael Steele. 1994. Le Cam's inequality and Poisson approximations. *The American Mathematical Monthly* 101, 1 (1994), 48–54.

[32] E. Summermatter and C. Grothoff. 2022. Byzantine Fault Tolerant Set Reconciliation. https://lsd.gnunet.org/lsd0003/.

[33] Massimiliano Taverna and Kenneth G Paterson. 2023. Snapping snap sync: practical attacks on go Ethereum synchronising nodes. In *32nd USENIX Security Symposium (USENIX Security 23)*. 3331–3348.

[34] Dennis Trautwein, Aravindh Raman, Gareth Tyson, Ignacio Castro, Will Scott, Moritz Schubotz, Bela Gipp, and Yiannis Psaras. 2022. Design and evaluation of IPFS: a storage layer for the decentralized web. In *Proceedings of the ACM SIGCOMM 2022 Conference*. 739–752.

[35] Jianguo Wang, Chunbin Lin, Yannis Papakonstantinou, and Steven Swanson. 2017. An experimental study of bitmap compression vs. inverted list compression. In *Proceedings of the 2017 ACM International Conference on Management of Data*. 993–1008.

[36] Gavin Wood. 2014. Ethereum: A secure decentralised generalised transaction ledger. (2014).

[37] Pieter Wuille. [n. d.]. Minisketch: a library for BCH-based set reconciliation. https://github.com/sipa/minisketch.

[38] Cong Yue, Zhongle Xie, Meihui Zhang, Gang Chen, Beng Chin Ooi, Sheng Wang, and Xiaokui Xiao. 2020. Analysis of indexing structures for immutable data. In *Proceedings of the 2020 ACM SIGMOD International Conference on Management of Data*. 925–935.

A ANALYSIS ON REGULAR IBLTS

We state and prove Theorems A.1 and A.2, which show that the efficiency of regular IBLTs degrades exponentially fast when being used to reconcile more or fewer differences than parameterized for. We state the theorems with respect to generic sets of source symbols. When using IBLTs for set reconciliation (§ 3), the sets are $A \triangle B$.

Theorem A.1. *For a random set of n source symbols and a corresponding regular IBLT with m coded symbols, the probability that the peeling decoder can recover at least one source symbol decreases exponentially in n/m.*

Proof. For the peeling decoder to recover at least one source symbol, there must be at least one pure coded symbol at the beginning. Otherwise, peeling cannot start, and no source symbol can be recovered. We now calculate a lower bound on the probability p_{nopure} that no pure coded symbol exists. Note that there is another parameter for regular IBLTs, k, which determines the number of coded symbols each source symbol is mapped to (§ 3). However, it can be shown that the probability that no pure coded symbol exists increases with k, so we set $k = 1$ to get a lower bound.

We consider the equivalent problem: if we throw n balls (source symbols) uniformly at random into m bins (coded symbols), what is a lower bound on the probability that no bin ends up having exactly one ball? We compute the number of ways f such that at least one bin has exactly one ball, which is the opposite of the event we are interested in. We set aside one of the m bins which will get exactly one ball, and assign one of the n balls to this bin. We then throw the remaining $n-1$ balls into the remaining $m-1$ bins freely. Notice that there are duplicates, so we get an upper bound

$$f \le mn(m-1)^{n-1}.$$

The total number of ways to throw n balls into m bins is

$$g = m^n.$$

Each way of throwing is equally likely to happen, so the probability p_{nopure} that no bin ends up with exactly one ball has a lower bound

$$\begin{aligned} p_{\text{nopure}} &= 1 - f/g \\ &\ge 1 - \frac{mn(m-1)^{n-1}}{m^n} \\ &= 1 - \frac{n(m-1)^{n-1}}{m^{n-1}} \\ &= 1 - n\left(1 - \frac{1}{m}\right)^{n-1} \end{aligned}$$

We are interested in the event where peeling can start, which is the opposite event. Its probability has an upper bound for $n/m > 1$

$$\begin{aligned} p_{\text{haspure}} &= 1 - p_{\text{nopure}} \\ &\le n\left(1 - \frac{1}{m}\right)^{n-1} \\ &\le ne^{-\frac{n-1}{m}} \\ &= o(1.5^{-\frac{n}{m}}). \end{aligned}$$

□

The following theorem says that when dropping a fraction of a regular IBLT to reconcile a smaller number of differences n with a constant overhead η (the ratio between the number of used coded symbols and the number of source symbols n), the success probability decreases quickly as a larger fraction gets dropped.

Theorem A.2. *Consider a random set of n source symbols and a corresponding regular IBLT with m coded symbols, where each source symbol is mapped to k coded symbols. The peeling decoder tries to recover all source symbols using the first ηn coded symbols. k and η are constants, and $\eta n \le m$. The probability that it succeeds decreases exponentially in $1 - \eta n/m$.*

Proof. For the peeling decoder to succeed, each of the source symbols must be mapped at least once to the first ηn coded symbols. Because each source symbol is uniformly mapped to k of the m coded symbols, the probability that one is only mapped to the remaining $m - \eta n$ coded symbols that the decoder does not use ("missed") is

$$\begin{aligned} p_{\text{missone}} &= \binom{m-\eta n}{k} \Big/ \binom{m}{k} \\ &= \frac{(m-\eta n)(m-\eta n-1)\dots(m-\eta n-k+1)}{m(m-1)\dots(m-k+1)} \\ &\approx \left(1 - \frac{\eta n}{m}\right)^k. \end{aligned}$$

The last step approximates $\frac{m-\eta n-k+1}{m-k+1}$ with $\frac{m-\eta n}{m}$. This does not change the result qualitatively because k is a constant.

The probability that no source symbol is missed is

$$\begin{aligned} p_{\text{nomiss}} &= (1 - p_{\text{missone}})^n \\ &\leq e^{-np_{\text{missone}}} \\ &= e^{-n\left(1-\frac{\eta n}{m}\right)^k}. \end{aligned}$$

□

B DERIVATION OF P_g AND $C(x)$

Here we calculate P_g and $C(x)$ as defined in § 4.2 when the parameter α in $\rho(i)$ is set to 0.5.

$$\begin{aligned} P_g &= (1-\rho(i+1))(1-\rho(i+2))\dots(1-\rho(i+g-1))\rho(i+g) \\ &= \frac{2}{i+g+2}\prod_{n=1}^{g-1}\frac{i+n}{i+n+2} \\ &= \frac{2}{i+g+2}\left(\prod_{n=1}^{g-1} i+n\right)\left(\prod_{n=3}^{g+1}\frac{1}{i+n}\right) \\ &= \frac{2(i+1)(i+2)}{(i+g)(i+g+1)(i+g+2)}. \end{aligned}$$

Before calculating $C(x)$, notice that

$$P_g = \frac{(i+1)(i+2)}{(i+g)(i+g+1)} - \frac{(i+1)(i+2)}{(i+g+1)(i+g+2)}.$$

We now calculate $C(x)$.

$$\begin{aligned} C(x) &= \sum_{g=1}^{x} P_g \\ &= \sum_{g=1}^{x}\left(\frac{(i+1)(i+2)}{(i+g)(i+g+1)} - \frac{(i+1)(i+2)}{(i+g+1)(i+g+2)}\right) \\ &= \sum_{g=1}^{x}\frac{(i+1)(i+2)}{(i+g)(i+g+1)} - \sum_{g=2}^{x+1}\frac{(i+1)(i+2)}{(i+g)(i+g+1)} \\ &= 1 - \frac{(i+1)(i+2)}{(i+x+1)(i+x+2)} \\ &= \frac{x(2i+x+3)}{(i+x+1)(i+x+2)}. \end{aligned}$$

C DEFERRED PROOFS

Lemma C.1 (Restatement of Lemma 4.1). *For any $\epsilon > 0$, any mapping probability $\rho(i)$ such that $\rho(i) = \Omega\left(1/i^{1-\epsilon}\right)$, and any $\sigma > 0$, if there exists at least one pure coded symbol within the first m coded symbols for a random set S with probability σ, then $m = \omega(|S|)$.*

Proof. We need to show $\forall\eta > 0\, \exists|S|_0 > 0\, \forall|S| > |S|_0 : m > \eta|S|$. Because $\rho(i) = \Omega\left(1/i^{1-\epsilon}\right)$, there exists $\delta > 0$ and $i_0 > 0$, such that $\rho(i) \geq \delta/i^{1-\epsilon}$ for all $i > i_0$. Let ρ_0 be the smallest non-zero value among $\rho(i)$ for all $0 \leq i \leq i_0$. Let

$$|S|_0 = \max\left(\left(\frac{\eta^{1-\epsilon}}{\delta}\right)^{\frac{1}{\epsilon}}, \frac{1}{\eta}\left(\frac{\delta}{\rho_0}\right)^{\frac{1}{1-\epsilon}}, |S|^*\right)$$

where $|S|^*$ is such that for all $|S| > |S|^*$,

$$e \cdot \delta\eta^\epsilon |S|^{1+\epsilon} \exp\left(-\frac{\delta|S|^\epsilon}{\eta^{1-\epsilon}}\right) < \sigma.$$

Note that $\exp\left(\frac{\delta|S|^\epsilon}{\eta^{1-\epsilon}}\right) = \omega\left(|S|^{1+\epsilon}\right)$, so such $|S|^*$ always exists.

For any $i \geq 0$, the i-th coded symbol is pure if and only if *exactly* one source symbol is mapped to it, which happens with probability

$$\begin{aligned} P_i &= |S|\rho(i)(1-\rho(i))^{|S|-1} \\ &\leq e \cdot |S|\rho(i)e^{-|S|\rho(i)}. \end{aligned}$$

The inequality comes from the fact that $(1-x)^y \leq e^{-xy}$ for any $0 \leq x \leq 1$ and $y \geq 1$.

By the definition of $|S|_0$, for any $|S| > |S|_0$ and any $0 \leq i \leq \eta|S|$, either $\rho(i) = 0$, or $\rho(i) \geq \frac{\delta}{(\eta|S|)^{1-\epsilon}}$ and $|S|\rho(i) > 1$. In either case,

$$P_i \leq e \cdot \frac{\delta|S|^\epsilon}{\eta^{1-\epsilon}} \exp\left(-\frac{\delta|S|^\epsilon}{\eta^{1-\epsilon}}\right).$$

Recall that we want at least one pure symbol among the first m coded symbols. Assume for contradiction that $m \leq \eta|S|$. Then, failure happens with probability

$$\begin{aligned} P_{\text{fail}} &= \prod_{i=0}^{m-1}(1-P_i) \\ &\geq \prod_{i=0}^{\eta|S|-1}(1-P_i) \\ &\geq \left(1 - e \cdot \frac{\delta|S|^\epsilon}{\eta^{1-\epsilon}} \exp\left(-\frac{\delta|S|^\epsilon}{\eta^{1-\epsilon}}\right)\right)^{\eta|S|} \\ &\geq 1 - e \cdot \delta\eta^\epsilon|S|^{1+\epsilon} \exp\left(-\frac{\delta|S|^\epsilon}{\eta^{1-\epsilon}}\right) \\ &> 1 - \sigma. \end{aligned}$$

□

We remark that a stronger result which only requires $\rho(i) = \omega(\log i/i)$ can be shown with a very similar proof, which we omit for simplicity and lack of practical implications. We may also consider a generalization of this lemma, by requiring there to be at least k coded symbols with at most k source symbols mapped to each, for every $k \leq |S|$. (Lemma 4.1 is the special case of $k = 1$.) This may lead to an even tighter bound on $\rho(i)$, which we conjecture to be $\rho(i) = \omega(1/i)$.

Lemma C.2 (Restatement of Lemma 4.2). *For any mapping probability $\rho(i)$ such that $\rho(i) = o(1/i)$, and any $\sigma > 0$, if there exist at least $|S|$ non-empty coded symbols within the first m coded symbols for a random set S with probability σ, then $m = \omega(|S|)$.*

Proof. We need to show that $\forall \eta > 0\, \exists |S|_0 > 0\, \forall |S| > |S|_0 : m > \eta|S|$. First, note that for there to be $|S|$ non-empty symbols within the first m coded symbols, m cannot be smaller than $|S|$, so the statement is trivially true for $0 < \eta < 1$. We now prove for the case of $\eta \geq 1$.

For any $\eta \geq 1$, let $\delta = \frac{1}{4\eta}$. Because $\rho(i) = o(1/i)$, there must exist $i_0 > 0$ such that $\rho(i) < \delta/i$ for all $i > i_0$. Let

$$|S|_0 = \max(2i_0, 4\eta^2(1-2\eta)\log(\sigma)).$$

For all $i \geq |S|/2$, the i-th coded symbol is non-empty with probability

$$\begin{aligned} P_i &= 1 - (1 - \rho(i))^{|S|} \\ &< 1 - \left(1 - \frac{2\delta}{|S|}\right)^{|S|} \\ &\leq 2\delta. \end{aligned}$$

The first inequality is because $\rho(i) < \delta/i$ for $i \geq |S|/2$, and the second inequality is because $(1-x)^y \geq 1 - xy$ for any $x < 1$ and $y \geq 1$.

In order to get $|S|$ non-empty symbols among the first m coded symbols, there must be at least $|S|/2$ non-empty symbols from index $i = |S|/2$ to index $i = m-1$. To derive an upper bond on this probability, we assume that each is non-empty with probability 2δ, which, as we just saw, is strictly an overestimate. By Hoeffding's inequality, the probability that there are at least $|S|/2$ non-empty symbols has an upper bound

$$P_{\text{succ}} < \exp\left((|S| - 2m)\left(2\delta - \frac{|S|}{2m - |S|}\right)^2\right)$$

when $m \leq (\frac{1}{4\delta} + \frac{1}{2})|S|$, which is true for all $m \leq \eta|S|$.

Assume $m \leq \eta|S|$ for contradiction. By the definition of δ, the previous upper bound becomes

$$P_{\text{succ}} < \exp\left(\frac{|S|}{4\eta^2(1-2\eta)}\right).$$

The right hand side monotonically decreases with $|S|$. So, by the definition of $|S|_0$, for all $|S| > |S|_0$,

$$P_{\text{succ}} < \exp\left(\frac{|S|_0}{4\eta^2(1-2\eta)}\right) \leq \sigma.$$

□

Theorem C.3 (Restatement of Theorem 5.1). *For a random set of n source symbols, the probability that the peeling decoder successfully recovers the set using the first ηn coded symbols (as defined in § 4) goes to 1 as n goes to infinity. Here, η is any positive constant such that*

$$\forall q \in (0, 1] : e^{\frac{1}{\alpha} Ei\left(-\frac{q}{\alpha\eta}\right)} < q.$$

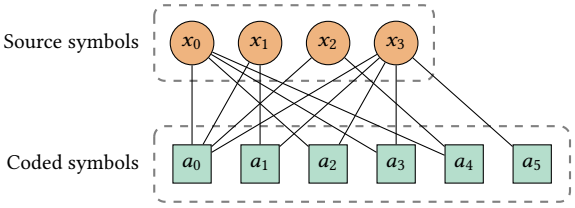

Figure 13: Example of the bipartite graph representation of a set of source symbols, x_0, x_1, x_2, x_3, and its first 6 coded symbols, $a_0, a_1, \ldots, a_5$.

Before proving the theorem, we introduce the graph representation of a set of source symbols and the corresponding coded symbols. Imagine a bipartite graph where each source or coded symbol is a vertex in the graph, and there is an edge between a source and a coded symbol if and only if the former is mapped to the latter during encoding. Fig. 13 is an example. We define the degree of a symbol as the number of neighbors it has in this bipartite graph, i.e., its degree as in graph theory. For example, in Fig. 13, source symbol x_0 has degree 4, and coded symbol a_1 has degree 2.

We also define the degree of an *edge* in the graph [14]. The *source degree* of an edge is the degree of the source symbol it connects to, and its *coded degree* is the degree of the coded symbol it connects to. For example, for the edge connecting x_3 and a_3 in Fig. 13, its source degree is 5 because x_3 has degree 5, and its coded degree is 2 because a_3 has degree 2.

We remark that density evolution is a standard technique [18, 29] of analyzing codes that are based on random graphs, such as LT [17] and LDPC [8] codes. Our proof mostly follows these analysis, in particular, [18, § 2]. However, the mapping probability $\rho(i)$ in Rateless IBLTs is a function whose parameter i goes to infinity as the set size goes to infinity. This is a key challenge that we solve in our analysis, which enables us to get the closed-form expression in Theorem 5.1.

Proof. Consider n random source symbols and its first m coded symbols. Let Λ be the random variable denoting the degree of a random source symbol. Let Λ_u $(0 \leq u \leq m)$ be the probability that Λ takes value u. Similarly, let Ψ be the random variable denoting the degree of a random coded symbol. Let Ψ_v $(0 \leq v \leq n)$ be the probability that Ψ takes value v. Define the probability generating functions of Λ and

Ψ,

$$\Lambda(x) = \sum_{u=0}^{m} \Lambda_u x^u,$$
$$\Psi(x) = \sum_{v=0}^{n} \Psi_v x^v.$$

We also consider the degree of a random edge. Let λ be the random variable denoting the source degree of a random edge. Let λ_u ($0 \le u \le m$) be the probability that λ takes value u. It is the fraction of edges with source degree u among all edges, i.e.,

$$\lambda_u = \frac{\Lambda_u u}{\sum_{w=0}^{m} \Lambda_w w} = \frac{\Lambda_u u}{\mathbb{E}(\Lambda)}.$$

Let $\lambda(x)$ be the generating function of λ, defined as

$$\lambda(x) = \sum_{u=0}^{m} \lambda_u x^{u-1} = \frac{1}{\mathbb{E}(\Lambda)} \sum_{u=0}^{m} \Lambda_u u x^{u-1} = \frac{\Lambda'(x)}{\mathbb{E}(\Lambda)}.$$

Similarly, let φ be the random variable denoting the coded degree of a random edge. Let φ_v ($0 \le v \le n$) be the probability that φ takes value v. It is the fraction of edges with coded degree v among all edges, i.e.,

$$\varphi_v = \frac{\Psi_v v}{\sum_{w=0}^{n} \Psi_w w} = \frac{\Psi_v v}{\mathbb{E}(\Psi)}.$$

Let $\varphi(x)$ be the generating function of φ, defined as

$$\varphi(x) = \sum_{v=0}^{n} \varphi_v x^{v-1} = \frac{1}{\mathbb{E}(\Psi)} \sum_{v=0}^{n} \Psi_v v x^{v-1} = \frac{\Psi'(x)}{\mathbb{E}(\Psi)}.$$

Let us now consider $\Psi(x)$. Recall that each of the n random source symbols is mapped to the i-th coded symbol independently with probability $\rho(i)$. The degree of the i-th coded symbol thus follows binomial distribution, which takes v with probability $\binom{n}{v}\rho^v(i)(1-\rho(i))^{n-v}$. Because we are interested in a random coded symbol, its index i takes $0, 1, \ldots, m-1$ with equal probability $1/m$. By the law of total probability,

$$\Psi_v = \frac{1}{m} \sum_{i=0}^{m-1} \binom{n}{v} \rho^v(i)(1-\rho(i))^{n-v}.$$

Plugging it into the definition of $\Psi(x)$, we get

$$\begin{aligned}\Psi(x) &= \sum_{v=0}^{n} \Psi_v x^v \\ &= \sum_{v=0}^{n} \frac{1}{m} \sum_{i=0}^{m-1} \binom{n}{v} \rho^v(i)(1-\rho(i))^{n-v} x^v \\ &= \frac{1}{m} \sum_{i=0}^{m-1} \sum_{v=0}^{n} \binom{n}{v} (x\rho(i))^v (1-\rho(i))^{n-v} \\ &= \frac{1}{m} \sum_{i=0}^{m-1} (1-(1-x)\rho(i))^n.\end{aligned}$$

Here, the last step is because of the binomial theorem. Plugging it into the definition of $\varphi(x)$, we get

$$\varphi(x) = \frac{n}{m\mathbb{E}(\Psi)} \sum_{i=0}^{m-1} \rho(i)(\rho(i)(x-1)+1)^{n-1}.$$

By the handshaking lemma, which says the sum of the degree of all source symbols should equal the sum of the degree of all coded symbols,

$$m\mathbb{E}(\Psi) = m \sum_{v=0}^{n} \Psi_v v = n \sum_{u=0}^{m} \Lambda_u u = n\mathbb{E}(\Lambda).$$

So, we can further simplify $\varphi(x)$ as

$$\varphi(x) = \frac{1}{\mathbb{E}(\Lambda)} \sum_{i=0}^{m-1} \rho(i)(\rho(i)(x-1)+1)^{n-1}.$$

Next, let us consider $\Lambda(x)$. For a random source symbol, it is mapped to the i-th coded symbol independently with probability $\rho(i)$. Its degree Λ is thus the sum of independent Bernoulli random variables with success probabilities $\rho(0), \rho(1), \ldots, \rho(m-1)$, which follows Poisson binomial distribution. By an extension [31, § 5] to Le Cam's theorem [16], we can approximate this distribution with a Poisson distribution of rate $\sum_{i=0}^{m-1} \rho(i)$, i.e., $\mathbb{E}(\Lambda)$, with the total variation distance between the two distributions tending to zero as m goes to infinity. That is,

$$\sum_{u=0}^{\infty} \left| \Lambda_u - \frac{(\mathbb{E}(\Lambda))^u e^{-\mathbb{E}(\Lambda)}}{u!} \right| < \frac{2}{\mathbb{E}(\Lambda)} \sum_{i=0}^{m-1} \rho^2(i).$$

When $\rho(i) = \frac{1}{1+\alpha i}$ for any $\alpha > 0$, the right hand side of the inequality goes to zero as m goes to infinity.

Recall that the probability generating function of a Poisson random variable with rate $\mathbb{E}(\Lambda)$ is

$$\Lambda(x) = e^{\mathbb{E}(\Lambda)(x-1)}.$$

Plugging it into the definition of $\lambda(x)$, we get

$$\lambda(x) = e^{\mathbb{E}(\Lambda)(x-1)}.$$

Let q denote the probability that a randomly chosen edge connects to a source symbol that is *not yet* recovered. As decoding progresses, q is updated according to the following function [14, 18]

$$\begin{aligned} f(q) &= \lambda(1-\varphi(1-q)) \\ &= e^{-\mathbb{E}(\Lambda)\varphi(1-q)} \\ &= e^{-\sum_{i=0}^{m-1}\rho(i)(1-q\rho(i))^{n-1}}. \end{aligned}$$

Let us consider $f(q)$ when the number of source symbols n goes to infinity, and the ratio of coded and source symbols is fixed, i.e., $\eta = m/n$ where η is a positive constant. Recall that $\rho(i) = \frac{1}{1+\alpha i}$. Notice that

$$e^{-\frac{nq}{\alpha i}} \leq (1-q\rho(i))^{n-1} \leq e^{-\frac{(n-1)q}{1+\alpha i}}$$

holds for all $n \geq 1$, $i \geq 0$, $\alpha > 0$, and $0 \leq q \leq 1$. We use this inequality and the squeeze theorem to calculate the limit of the exponent of $f(q)$ when n goes to infinity.

We first calculate the lower bound.

$$\begin{aligned} \lim_{n\to\infty} -\ln(f(q)) &= \lim_{n\to\infty} \sum_{i=0}^{\eta n-1} \rho(i)(1-q\rho(i))^{n-1} \\ &\geq \lim_{n\to\infty} \sum_{i=0}^{\eta n-1} \rho(i) e^{-nq/(\alpha i)} \\ &= \lim_{n\to\infty} \sum_{i=0}^{\eta n-1} \frac{1}{(1+\alpha i)e^{nq/(\alpha i)}} \\ &= \lim_{n\to\infty} \frac{1}{n} \sum_{i=0}^{\eta n-1} \frac{1}{(\frac{1}{n}+\alpha\cdot\frac{i}{n})e^{\frac{q}{\alpha}\cdot\frac{n}{i}}} \\ &= \int_0^{\eta} \frac{1}{\alpha x e^{\frac{q}{\alpha x}}} dx \\ &= -\frac{1}{\alpha}\mathrm{Ei}\left(-\frac{q}{\alpha\eta}\right). \end{aligned}$$

Here, $\mathrm{Ei}(\cdot)$ is the exponential integral function.

We then calculate the upper bound.

$$\begin{aligned} \lim_{n\to\infty} -\ln(f(q)) &= \lim_{n\to\infty} \sum_{i=0}^{\eta n-1} \rho(i)(1-q\rho(i))^{n-1} \\ &\leq \lim_{n\to\infty} \sum_{i=0}^{\eta n-1} \rho(i) e^{-\frac{(n-1)q}{1+\alpha i}} \\ &= \lim_{n\to\infty} \sum_{i=0}^{\eta n-1} \frac{1}{(1+\alpha i)e^{\frac{(n-1)q}{1+\alpha i}}} \\ &= \lim_{n\to\infty} \frac{1}{(n-1)q} \sum_{i=0}^{\eta n-1} \frac{1}{\frac{1+\alpha i}{(n-1)q} e^{\frac{(n-1)q}{1+\alpha i}}} \\ &= \frac{1}{\alpha}\int_0^{\alpha\eta/q} \frac{1}{xe^{1/x}} dx \\ &= -\frac{1}{\alpha}\mathrm{Ei}\left(-\frac{q}{\alpha\eta}\right). \end{aligned}$$

By the squeeze theorem,

$$\lim_{n\to\infty} -\ln(f(q)) = -\frac{1}{\alpha}\mathrm{Ei}\left(-\frac{q}{\alpha\eta}\right).$$

Plugging it into $f(q)$, we have

$$\lim_{n\to\infty} f(q) = e^{\frac{1}{\alpha}\mathrm{Ei}\left(-\frac{q}{\alpha\eta}\right)}.$$

By standard results [18, § 2][14, § III.B] of density evolution analysis, if

$$f(q) < q$$

holds for all $q \in (0, 1]$, then the probability that all source symbols are recovered when the decoding process terminates tends to 1 as n goes to infinity. Plugging in the closed-form result of $\lim_{n\to\infty} f(q)$, we get the condition

$$e^{\frac{1}{\alpha}\mathrm{Ei}\left(-\frac{q}{\alpha\eta}\right)} < q,$$

which should hold for all $q \in (0, 1]$ for the success probability to converge to 1. □

We refer readers to the literature [18] for a formal treatment on density evolution, in particular the result [18, § 2.2] that $\forall q \in (0, 1] : f(q) < q$ is a sufficient condition for the success probability to converge to 1, which we use directly in our proof. Here, we give some intuition. Recall that q is the probability that a random edge in the bipartite graph connects to a source symbol that is *not yet* recovered. Let p be the probability that a random edge connects to a coded symbol that is *not yet* decoded, i.e., has more than one neighbors that are not yet recovered. Density evolution iteratively updates q and p by simulating the peeling decoder. For a random edge with source degree u, the source symbol it connects to is not yet recovered if none of the source symbol's other $u-1$ neighbors is decoded. This happens with probability

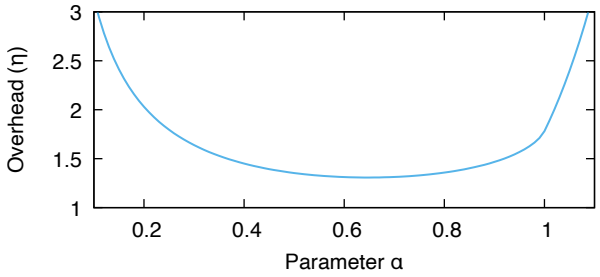

Figure 14: Relationship between the communication overhead and the parameter α.

p^{u-1}. Similarly, for a random edge with coded degree v, the coded symbol it connects to is not decoded if not all of the coded symbol's other $v-1$ neighbors are recovered. This happens with probability $1-(1-q)^{v-1}$.

Because q and p are the probabilities with regard to a random edge, we take the mean over the distributions of source and coded degrees of the edge, and the results are the new values of q and p after one iteration of peeling. In particular, in each iteration [14, 18],

$$p \leftarrow \sum_v \varphi_v \left(1-(1-q)^{v-1}\right),$$
$$q \leftarrow \sum_u \lambda_u p^{u-1}.$$

By the definition of the generating functions of φ and λ, the above equations can be written as

$$p \leftarrow 1-\varphi(1-q),$$
$$q \leftarrow \lambda(p).$$

Combine the two equations, and we get

$$q \leftarrow \lambda(1-\varphi(1-q)).$$

Notice that its right hand side is $f(q)$. Intuitively, by requiring $f(q) < q$ for all $q \in (0,1]$, we make sure that the peeling decoder always makes progress, i.e., the non-recovery probability q gets smaller, regardless of the current q. Conversely, if the inequality has a fixed point q^* such that $f(q^*) = q^*$, then the decoder will stop making progress after recovering $(1-q^*)$-fraction of source symbols, implying a failure.

D ADDITIONAL ANALYTICAL RESULTS

Theorem 5.1 shows the relationship between α, the parameter in the mapping probability function $\rho(i) = \frac{1}{1+\alpha i}$, and the communication overhead. For any α, the overhead η^* is the smallest η that satisfies Eq. 2. Fig. 14 shows the relationship between α and η^*.

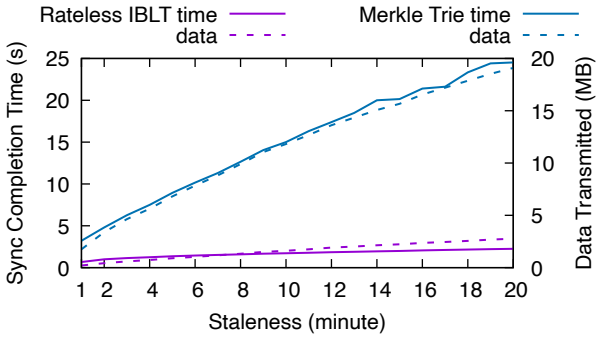

Figure 15: Completion time and communication cost when synchronizing Ethereum ledger states at different staleness over a network link with 50 ms of propagation delay and 20 Mbps of bandwidth.

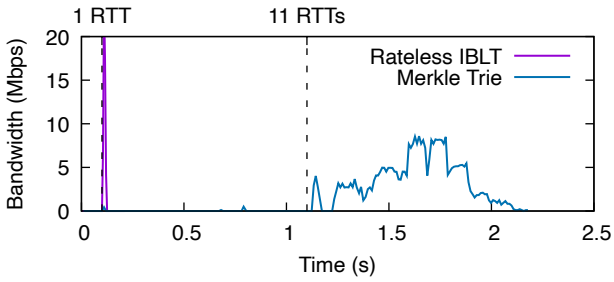

Figure 16: Time series of bandwidth usage when synchronizing Ethereum ledger states that are 1 block (12 seconds) stale. The network link has 50 ms of propagation delay and 20 Mbps of bandwidth. Time starts when Bob sees the TCP socket open.

E ADDITIONAL EVALUATION RESULTS

Fig. 15 complements Fig. 11 (§ 7.3). It shows the completion time and communication cost when synchronizing a smaller ledger state difference. Rateless IBLT achieves 4.8–10.9× lower completion time than state heal, and 6.9–8.6× lower communication cost.

Fig. 16 shows traces of bandwidth usage when synchronizing one block worth of state difference (see § 7.3 for the setup). For Rateless IBLT, the first coded symbol arrives at Bob in 1 round-trip time (RTT) after his TCP socket opens (0.5 RTT for TCP `ACK` to reach Alice, and another 0.5 RTT for the first symbol to arrive). Subsequent symbols arrive at line rate, as the peak at 1 RTT indicates. In comparison, for state heal, Alice and Bob reach the bottom of their tries after 11 RTTs; before that, they do not know the actual key-value pairs that differ, and the network link stays almost idle.